Trapeze Instability as a Source of Internal Gravity Waves. Part I

ISIDORO ORLANSKI

Geophysical Fluid Dynamics Laboratory, NOAA, Princeton University, Princeton, N. J. 08540

(Manuscript received 24 October 1972, in revised form 27 April 1973)

ABSTRACT

We can identify the diurnal oscillation of the atmospheric boundary layer as an important source of mesoscale internal gravity waves in the lower atmosphere.

The oscillation period of these waves is a function of latitude. A definitive two-day period may be found in the equatorial regions with scales on the order of a few hundred kilometers. In particular, for a situation in which the mean stratification at any time of the day is unstable, the wavelength could be on the order of 100 km. This result suggests that some cloud clusters may be originated by this process.

1. Introduction

Most of the energy in meso or smaller scales is due to internal gravity waves in the free atmosphere and and it has been recognized that they play a major role in the dynamics of such scales (Lilly, 1972). Through interaction with the mean ambient conditions, they remove energy from the larger scales and are the mechanisms by which energy is transported to smaller and smaller scales. In addition, they can trigger local storms, produce cloud clusters a hundred times the scale of a single cloud, maintain a large-scale jet due to some absorption mechanisms (Bretherton, 1969), or produce turbulence in remote places from the input source of energy (Gossard *et al.*, 1970). Obviously, it is important to try to identify all the mechanisms that can generate such waves. Most of them are well known but they are very localized. It is known that internal gravity waves will be generated by:

1) Shear unstable flows. If the unstable-shear effect overcomes the stabilizing-buoyancy effect due to stratification, the process is primarily important for generating Kelvin-Helmholtz waves in the atmosphere with scales smaller than 100 km (Scorer, 1969).

2) Convective cells penetrating into the stable atmosphere. This process is equally important for generating internal gravity waves and again the scales are on the order of a few tens of kilometers (Deardorff *et al.* 1969).

3) Large storm systems, fronts, hurricanes, etc. The generation of internal gravity waves by these mechanisms occurs in a manner similar to that stated above (Orlanski, 1968).

4) The topographic boundary, variable flows over mountains, land-sea contrast, etc. These processes are perhaps the most obvious ones for generating internal gravity waves (Lilly, 1972).

In this paper I would like to present a different and perhaps more general source of internal gravity waves in the atmosphere, since we will consider a global source rather than local sources as mentioned above.

In recent papers, Venezian (1969), Yih and Li (1972), etc., the effects of unsteady flows on convective instability are discussed. It has been determined that if the fluid is gravitationally unstable and oscillatory in time, the familiar convective instability which develops in such a flow can be modified so that it is either reinforced or dampened with control being exerted by such parameters as the oscillation frequency and the unstable lapse rate of the fluid. The equations describing the dynamics of this flow are the Mathieu equations which are well known in physics and astronomy. References to these equations in fluid dynamics can be seen in Yih and Li (1972).

Let us discuss a problem closely related to those previously mentioned; however, the primary difference between this work and the others is that in this one the effect of oscillatory behavior in stable rather than unstable systems will be considered. This case has profound implications in the dynamics of the atmosphere, particularly in regions where large portions of the atmosphere have a persistent oscillation. The diurnal boundary layer for the lower atmosphere and the ozone layer in the upper atmosphere are two such examples.

It is well known that the diurnal temperature variation near the ground produces a noticeable effect in the lowest kilometer of the atmosphere. In the daytime when maximum heating occurs, strong convective cells are generated in the lower hundred meters which then rise by buoyancy, thus penetrating the stable layers of the atmosphere to an order of a few kilometers. In this process the heat exchange modifies the stable lapse rates encountered at those altitudes to a neutral one.

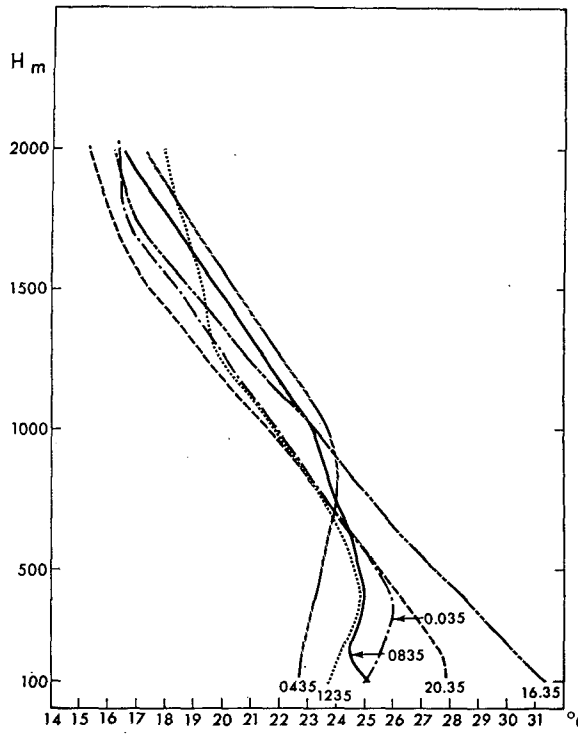

FIG. 1. Characteristic profiles of atmospheric temperature for different times of the day as a function of height. (After Lettau and Davidson, 1957.)

[Fig. 1 shows the temperature for different times of the day (after Lettau and Davidson, 1957).] This process continues until sunset when turbulence due to convective instability decays. Since the ground as well as the lowest layers of the atmosphere cool due to radiation, the lapse rate is effectively increased to a more stable value. On the average we might say that the lower atmosphere is characterized by a static stability that oscillates with a diurnal period. If we define θ to be the potential temperature, then for the boundary layer we can write

$$\theta_z=\theta_{0z}+\theta_{1z}\cos\omega_0 t,$$

where $\theta_{0z}>\theta_{1z}>0$ and ω_0 is the diurnal frequency. In general, for mean average values the atmosphere will be statically stable but obviously less stable during the day than at night.

On the other hand, at an altitude of 40 km the diurnal variation of temperature is mainly due to the absorption of heat by ozone. In this case the system is also statically stable with a strong diurnal component (Chapman and Lindzen, 1970).

The response in a stable atmosphere is oscillatory motions called internal gravity waves. Our main concern is to look at the modification of such waves when an oscillatory part is included in the main stratification. We know that other variables such as the wind may also have an oscillatory behavior. However, the convective cells that are responsible for heat transfer are not directly connected with momentum transfer and I believe that the oscillatory behavior of the wind will occur as a result of the wave generation we intend to discuss here. Although we are considering a stable lapse rate at any time, the waves could become unstable. Before discussing the mechanism of this instability, let me describe a simple experiment which will clarify the concept.

Almost everyone knows that a trapezist moves his body harmonically to increase the amplitude of the trapeze oscillation; the same is true of a child using a swing. In both cases a constant increase in the total energy system is expected from the input work done by periodically changing the radius from the center of gravity to the support of the trapeze or swing. In a more physical experiment, we can describe the trapeze or swing as a pendulum of variable length (Fig. 2) in which the pendulum with length l is supported by a pulley (at a) and the string is connected to a motor. When the motor is turned off, the pendulum will oscillate with a frequency $\omega=(g/l_0)^{\frac{1}{2}}$, where g is gravity and l_0 the mean length of the string from a to o; the system thus obeys the equation for the displacement of the pendulum:

$$\ddot{X}+\frac{g}{l_0}X=0.$$

If we turn on a motor that rotates with a frequency of ω_0 and the radius b of the driver wheel is far smaller than l_0, the above equation to the first order is

$$\ddot{X}+\frac{g}{l_0}\left(1-\frac{b}{l_0}\cos\omega_0 t\right)X=0.$$

This is the Mathieu equation which for certain values of ω_0 and b/l_0 becomes unstable, or in this case is in

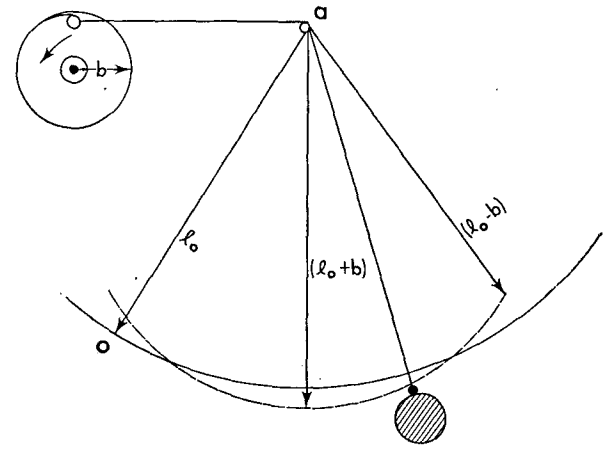

FIG. 2. A schematic diagram of a pendulum with a variable length. The amplitude of the variable length pendulum is given by the radius b of the driver wheel. The pendulum is supported by a pulley at a.

resonance. From the theory of the Mathieu equations it is known that the first instability will occur if $4g/(l_0\omega_0^2)\approx 1$ which is equivalent to saying that the system will be in resonance if the frequency of the pendulum is equal to $\frac{1}{2}$ the frequency of the forcing. As we shall see later, this is a very important result which we will apply to unstable internal gravity waves in the atmosphere. The mathematical discussion of Mathieu equations can be found in many text books (e.g., Morse and Feshback, etc.). It is noteworthy to say that the next unstable solution occurs when the frequency of the pendulum equals the frequency of the forcing. In fact, the infinite unstable branches of the Mathieu equations could be described as exponential growing solutions with frequencies that are multiples of $\omega_0/2$ or ω_0.

As mentioned earlier, the application of these equations to the atmospheric case will allow us to consider a new type of instability (trapeze instability) that could have primary importance with respect to the diurnal variation of the atmosphere.

2. The equations for an unsteady flow

We assume that the atmosphere has a lapse rate that is periodically modified by a non-specific process (small-scale convection, radiation or absorption, etc.), homogeneous in the horizontal spaces, and in constant rotation with angular velocity $f/2$. For simplicity let us consider the case without wind. Then the linear equations that describe the dynamics of very small disturbances are given by the anelastic equations:

$$\beta(U_t-fV)=-\theta_0\pi_x, \tag{2.1}$$

$$\beta(V_t+fU)=-\theta_0\pi_y, \tag{2.2}$$

$$\beta W_t=-\theta_0\pi_z+\beta\theta, \tag{2.3}$$

$$(\rho_0U)_x+(\rho_0V)_y+(\rho_0W)_z=0, \tag{2.4}$$

$$\theta_t+W\bar{\theta}_z=0, \tag{2.5}$$

where U, V, W are the x, y, z velocity components; π is the non-dimensional pressure $(P/p_0)^\chi$, where p_0 is the reference pressure and $\chi=R/C_p$; θ is the perturbation of the potential temperature $[=T/(\theta_0\pi)]$; ρ_0 is the reference density; and $\beta=gd/(C_P\theta_0)$.

From the horizontal divergence of (2.1) and (2.2) combined with the equation of the vertical vorticity components, we obtain an equation for the vertical velocity and π:

$$\beta(\rho_0W)_{zll}+\beta f^2(\rho_0W)_z=\rho_0\theta_0\nabla^2{}_H\pi_t. \tag{2.6}$$

We now differentiate (2.3) with respect to time and substitute θ_t from (2.5) to obtain

$$\beta\rho_0W_{ll}=-\rho_0\theta_0\pi_{zl}-\beta g\rho_0W\bar{\theta}_z, \tag{2.7}$$

and differentiate (2.6) with respect to z and take the horizontal Laplacian of (2.7). Combining both, we finally have

$$\left(\frac{\partial}{\partial z}-\frac{\rho_{0z}}{\rho_0}\right)(W'_{llz}+f^2W'_z)+\nabla^2_H(W'_{ll}+N^2W')=0, \tag{2.8}$$

where W' is the reference density multiplied by the vertical velocity ($W'=\rho_0W$) and N is the Brunt-Väisälä frequency ($N^2=+g\theta z/\theta_0$). Notice that $\rho_0/\rho_{0z}=H=C_pH_0/g$ is the depth of an insentropic atmosphere ($\sim$30 km); thus, for the motions with a vertical scale smaller than H in which we are interested, Eq. (2.8) can be simplified as follows:

$$W_{llzz}+f^2W_{zz}+\nabla_H{}^2[W_{ll}+N^2(z,t)W]=0. \tag{2.9}$$

It should be understood that from here on that $W=W'$. In the next two sections a discussion of the solution of (2.9) for different configurations of $N^2(z,t)$ will be treated.

3. Single stratified layer

We shall now discuss the response of the boundary layer with parameter characteristic of the atmospheric case; that is, a height of 1 km and a Brunt-Väisälä frequency defined as $N=(N_0{}^2+N_1{}^2\cos\omega_0t)^{\frac{1}{2}}$, where $N_0{}^2$ and $N_1{}^2$ are constant in height and are such that $N_0{}^2+N_1{}^2=N^2_{\text{night}}\approx 10^{-4}\ \text{sec}^{-2}$ and $N_0{}^2-N^2_{\text{day}}\epsilon>0$. In this case Eq. (2.9) can be written as

$$w_{llzz}+f^2w_{zz}-(k^2+l^2)\times[w_{ll}+(N_0{}^2+N_1{}^2\cos\omega_0t)w]=0, \tag{3.1}$$

where w is now a single horizontal Fourier component $\{W=\sum w_{k,l}\exp[i(k_x+l_y)]\}$. The boundary conditions for this simple case are that the vertical velocity equals zero at the ground and at the top of the boundary layer. In the next section, however, we will remove these artificial constraints. Since N^2 is independent of z, a solution which satisfies the boundary conditions will be

$$w=W_0\sin[m\pi/h)z]. \tag{3.2}$$

Substituting this equation in (3.1), we obtain

$$w_{0ll}+\left[\frac{(k^2+l^2)N_0{}^2+(m\pi/h)^2f^2}{k^2+l^2+(m\pi/h)^2}+\frac{(k^2+l^2)N_1{}^2}{k^2+l^2+(m\pi/h)^2}\cos\omega_0t\right]w=0. \tag{3.3}$$

If we redefine new parameters

$$\left.\begin{aligned} t&=\frac{2T}{\omega_0},\quad a=\frac{4}{\omega_0{}^2}\frac{(k^2+l^2)N_0{}^2+(m\pi/h)^2f^2}{[k^2+l^2+(m\pi/h)^2]}\\ q&=-\frac{2(k^2+l^2)N_1{}^2}{\omega_0{}^2[k^2+l^2+(m\pi/h)^2]}\end{aligned}\right\}, \tag{3.4}$$

Eq. (3.3) is transformed into a Mathieu equation

$$w_{TT}+(a-2q\cos 2T)w=0, \tag{3.5}$$

whose general solution is

$$w=C_1e^{\mu T}\phi(T)+C_2e^{-\mu T}\phi(-T). \tag{3.6}$$

Here $\phi(T)$ is a periodic function and μ could be complex (the general solution is obtained by the Floquet theorem) depending on the values of a and q. Our interest is to show for certain values of a and q that μ is real and allows for unstable solutions. Unfortunately, it is very difficult to find roots of μ; however, since $\phi(T)$ is periodic, it can be decomposed into Fourier components. Thus by substituting into (3.5), an infinite set of algebraic equations can be obtained for the Fourier coefficients. This homogeneous system defines an infinite determinant called a Hill determinant which is convergent. The roots of the determinant are a solution for μ as a function of a and q. Zaroodny (1955) numerically computed the growth rate as a function of a and q for the first unstable branches; these are shown in Fig. 3. Through our definition, the physical parameters are related to a and q as follows:

$$\left.\begin{aligned}\frac{2q}{a}&=\frac{(k^2+l^2)N_1^2}{(k^2+l^2)N_0^2+(m\pi/h)^2f^2}\\ a^{\frac{1}{2}}&=\frac{2}{\omega_0}\left[\frac{(k^2+l^2)N_0^2+(m\pi^2/h)f^2}{k^2+l^2+m\pi^2/h}\right]^{\frac{1}{2}}\end{aligned}\right\}. \tag{3.7}$$

Before discussing the physical implications of this instability, let us briefly examine Fig. 3. It is only the first four branches in which the growth rate has a positive real part. The contour lines where the growth rate equals zero define periodic solutions known as Mattieu functions. It is of particular interest to note that the maximum growth rate in each branch increases with $a^{\frac{1}{2}}$ when values of $-2q/a>1$. For values of $-2q/a<1$, the maximum growth rate decreases with a and reaches a maximum when a is close to 1. We will relate these differences to two processes that excite those instabilities. Let me simplify the discussion by considering the case where $f=0$. Then

$$-2q/a=N_1^2/N_0^2, \tag{3.8}$$

$$a^{\frac{1}{2}}=\frac{2}{\omega_0}\left[\frac{(k^2+l^2)N_0^2}{(k^2+l^2+2m\pi/h}\right]^{\frac{1}{2}}. \tag{3.9}$$

If we are looking for values of $-2q/a>1$, the implication is that $N_1^2>N_0^2$ which corresponds to the case for certain times of the day when the system has an unstable lapse rate or the Brunt-Väisälä frequency is imaginary. This type of convectively unstable system was discussed by Yih and Li (1972) and, as stated earlier, the growth rate for the inviscid case that we are treating will not have a cutoff wavelength; i.e., the growth rate will become larger as the wavenumbers become larger. However, our interest will be focused on the second process where $N_0^2>N_1^2$, $-2q/a<1$. We must remember that this case always corresponds to stable lapse rates. Nevertheless, the system does become unstable for values of a close to 1. In this case

$$\left[\frac{(k^2+l^2)N_0^2}{k^2+l^2+(m\pi/h)^2}\right]^{\frac{1}{2}}\approx\frac{\omega_0}{2}.$$

This result is of primary significance since the left-hand term represents the frequency of internal gravity waves in the absence of forced oscillation, and the above condition states that wave frequencies which are half the forcing frequency cause the system to be unstable. This instability has a large horizontal wavelength. For example, if N_0 is on the order of 10^{-2} sec^{-1} and h is 2000 m, then in the boundary layer case where $T_0=1$ day, the horizontal wavelength will be $\lambda\approx 600$ km. For the most unstable waves the period will be 2 days and the growth rate will be about $\mu\approx 0.628/T_0$. Our analysis thus far has been carried out using a model with an unrealistic boundary condition; however, the next section will show that considering a more realistic situation will render similar results. The difference in the latter case lies in the fact that the unstable wave covers the entire atmosphere rather than the boundary layer alone. In view of this, I should mention that a very similar type of wave was found in the equatorial regions by Murakami (1972). In his case, he stated that there is a definitive wave in the equatorial regions which has a wavelength of the order 1000 km and a period of about 2.5 days. If we remove the Doppler shift produced by the mean wind ($U\approx -5$ m sec^{-1}) at the observation time, the period and the 600-km horizontal scales of the waves are in very close agreement with those discussed here.

In concluding this section let us discuss the case where $f\neq 0$. The expressions for a and $-2q/a$ in this case are

$$\left.\begin{aligned}a&=\frac{4}{\omega_0^2}\frac{(k^2+l^2)N_0^2+(m\pi/h)^2f^2}{(k^2+l^2)+(m\pi/h)^2}\\ \frac{-2q}{a}&=\frac{(k^2+l^2)N_1^2}{(k^2+l^2)N^2+(m\pi/h)^2f^2}\end{aligned}\right\}. \tag{3.10}$$

It is easy to see for given values of k, l and m that there is a unique relation between a and $-2q/a$:

$$\frac{-2q}{a}=\frac{\epsilon(a-16\sin^2\theta)}{a[1-(4\omega_0^2/N_0^2)\sin^2\theta]}. \tag{3.11}$$

In this case f was replaced by $f=2\omega_0\sin\theta$ and N_1^2 by ϵN_0^2. Knowing that $N_0^2\gg f^2$ results in a further simplification of (3.11):

$$\frac{-2q}{a}=\frac{\epsilon}{a}(a-16\sin^2\theta). \tag{3.12}$$

We can see that at the equator ($f=0$)

$$-2q/a=\epsilon=N_1^2/N_0^2,$$

and the relation is in agreement with (3.8). Since trapeze instability requires that $(-2q/a)$ be larger than zero, it is possible to conclude from (3.12) that the possible values of a are those larger than

$$a_c=16\sin^2\theta.$$

In addition, the two main conclusions which can be drawn from (3.12) concerning the behavior of the trapeze instability at middle latitudes are that 1) only the branches with large a's are possible; and that 2) for a given a the parameter $-2q/a$ will decrease with increasing latitude (indicating a stabilization effect due to the earth's rotation).

4. Diurnal boundary layer of the atmosphere

If we remove the constraint of the top of the boundary layer considering that a free stable layer is on top of it, the problem becomes more difficult and non-separable in z and t. However, Eq. (3.1) still describes the system if we consider that

$$\left.\begin{aligned} N^2&=N_F^2(z), && \text{if } h<z<H\\ N^2&=N_1^2(z)+N_2^2(z)\cos\omega_0 t, && \text{if } 0<z<h \end{aligned}\right\}, \quad (4.1)$$

and numerically integrate (3.1) as a function of z and t.

The numerical integration was carried out to an altitude of $H=10{,}000$ m (with an equally spaced grid, $\Delta z=50$ m), using $h=1000$ m as the height of the boundary layer, and over 20 days (with a time step of $\Delta t=120$ sec).

The numerical method used to integrate (3.1) with boundary conditions (4.1) involved a function ϕ such that

$$\phi=w_{tt}+f^2w. \quad (4.2)$$

Using (4.2) on (3.1), we have

$$\phi_{zz}-\nabla_H^2\phi+\nabla_H^2[N^2(z,t)-f^2]w=0. \quad (4.3)$$

The boundary condition at $z=0$ is $w=0$ or $\phi(0)=0$ at $z=H$. Since we must prescribe a boundary condition for the numerical integration, we will consider two different cases: A, a rigid lid where $\phi(H)=0$ at $z=H$; and, B, $\phi_{zz}(H)=0$ at $z=H$.

a. A rigid lid at the top of the tropopause: Case A

This unrealistic boundary condition will affect high-frequency waves; however, the boundary condition is quite reasonable for waves with periods on the order of 1 day or more. Although some unrealistic reflection will occur due to the boundary condition, it would take about 10–20 days for the results in the lower boundary layer to be affected. This is the time required for waves generated in the lower boundary layer to propagate to the free atmosphere and be reflected. The solution

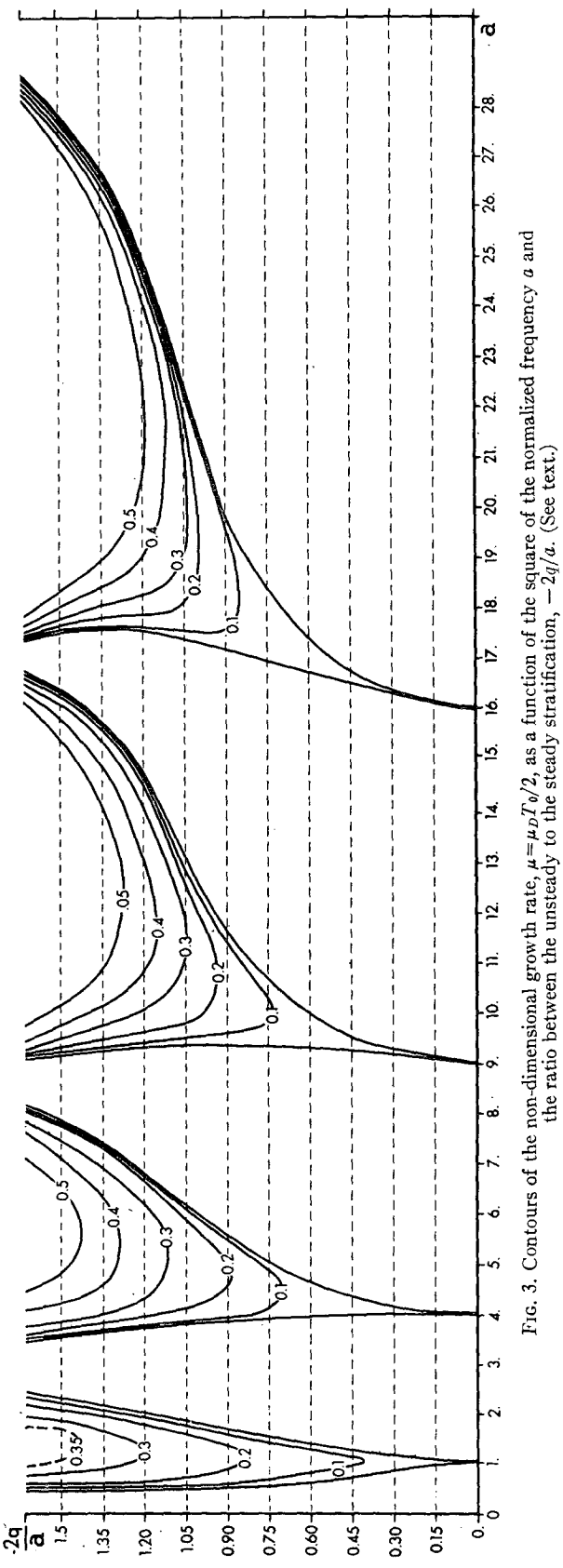

FIG. 3. Contours of the non-dimensional growth rate, $\mu=\mu_D T_0/2$, as a function of the square of the normalized frequency a and the ratio between the unsteady to the steady stratification, $-2q/a$. (See text.)

clearly shows that the waves in the lower atmosphere are growing exponentially due to the instability source in the boundary layer sooner before any effects from the reflected waves are noticeable. In this case the boundary conditions are

$$\phi(0)=0 \text{ and } \phi(H)=0. \tag{4.4}$$

Since (4.3) does not involve any time derivative of ϕ, given w and N^2 at each time, we obtain ϕ by integrating (4.3) in z by a recursive method (Richtmyer and Morton, 1967), using the boundary conditions of (4.4). By utilizing a central difference method for the time integration of (4.2), we obtain the vertical velocity

$$w^n=(2-\Delta t^2 f^2)w^n-w^{n-1}+\Delta t^2\phi^n, \tag{4.5}$$

where the superscript n determines the time integrations and Δt is the time step ($t=n\Delta t$). Initially we perturb the vertical velocity field, say by

$$w(z,0)=w_0 \sin[(n\pi/H)z], \tag{4.6}$$

where $w_0=10^{-4}$ in non-dimensional units and $n=10$.

As an example I will only show a few different integrations of this instability and its behavior with different parameters. I do not want to extrapolate the quantitative results since the model itself is very simple. However, in Part II (Orlanski, 1973) a complete discussion of this new instability will be presented, showing how much it is affected by a mean geostrophic shear flow.

Figs. 4–8 represent the computed dimensionless amplitude of the vertical velocity as a function of height and time. The different parameters which were used for each figure are shown in Table 1 and it should also be mentioned that the graphs show the case for the most unstable wavelength. Also, in each case we start with the vertical velocity that has already been described in (4.6) i.e., $n=10$.

The main difference between Figs. 4 and 5 is that Fig. 4 has a neutral stratification ($N_1=N_2$) during the day but in Fig. 5 the stratification is weakly stable ($N_1=1.1N_2$). We can identify these parameters with the graph in Fig. 3 in which we see that the case in Fig. 4 has a value of $2q/a$ greater than that in Fig. 5 and also that the system is more unstable (note that in Fig. 4 the contour interval is five times larger than that of Fig. 5).

Figs. 6 and 7 are similar but the difference lies in the fact that the horizontal wavelength is 805 km in Fig. 6, and 628 km in Fig. 7 which corresponds to a maximum instability; thus the two cases illustrate stable and unstable situations. Comparing the values of a in Fig. 3 shows that $a=0.74$ for Fig. 6 corresponding to the case of neutral stability and $a=0.94$ in Fig. 7 which is very close to the maximum growth rate. Note that while the Coriolis parameter is very small, 10^{-5} sec^{-1}, the solution still has a period of 2 days.

Since f is very small, the main difference between Figs. 4 and 7 is that the depth of the boundary layer in Fig. 7 is three times larger than that of Fig. 4, thus explaining the difference in the wavelength of the most unstable wave. We can also notice in comparing these two figures that they both have the same initial condi-

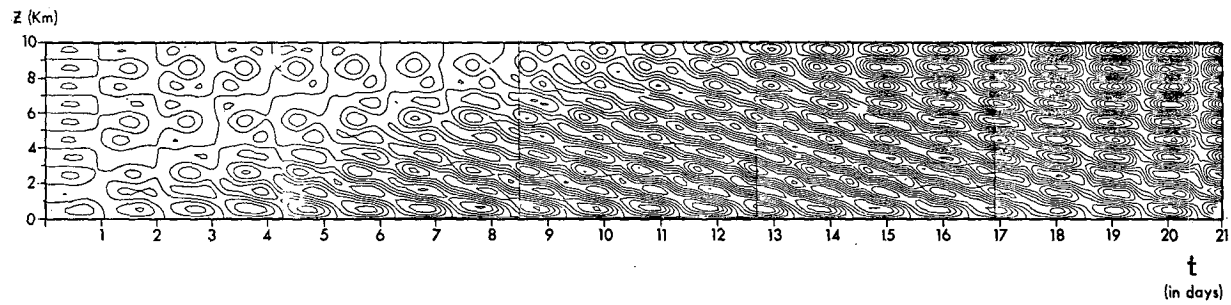

FIG. 4. Contours of the non-dimensional vertical velocity as a function of height and time. The parameters are specified in Case 1 of Table 1 and the contour interval is 0.01.

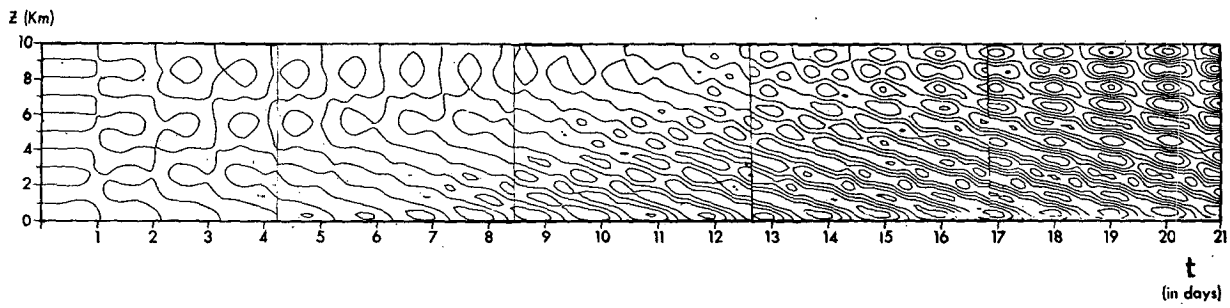

FIG. 5. As in Fig. 4 except for Case II and a contour interval of 0.02.

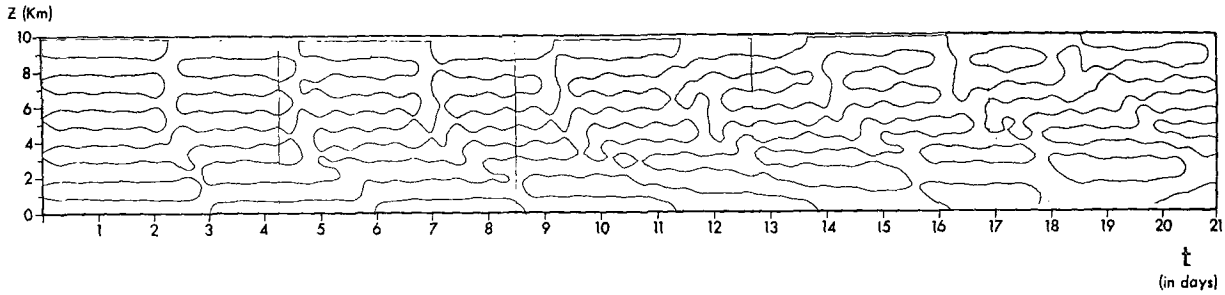

FIG. 6. As in Fig. 4 except for Case III and a contour interval of 0.05.

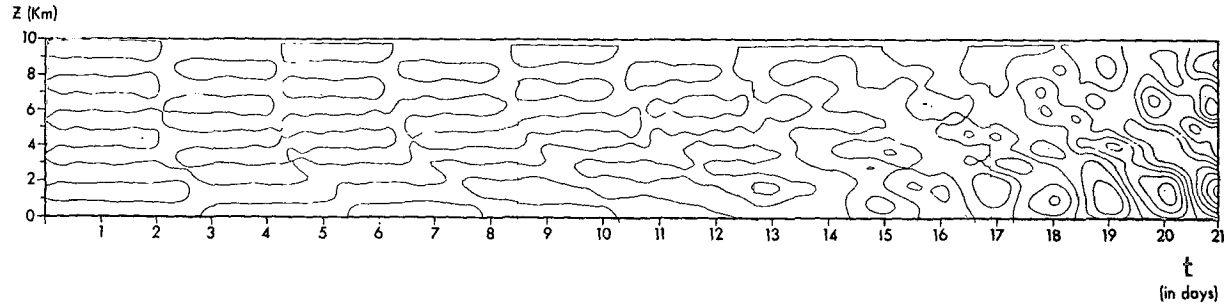

FIG. 7. As in Fig. 4 except for Case IV and a contour interval of 0.05.

tions; however, the depth of the cells is determined mainly by the depth of the boundary layer.

In Fig. 8 the solution is a little different. There, as we discussed in a previous section, the Coriolis force has an important stabilizing effect and does not allow solutions greater than 1 pendulum day. In this case the instability chooses another branch and, as we see in Fig. 3, it is closer to $a=3.0$. This is characteristic of higher frequencies and generally the frequency of the solution will be $3\omega_0/2$. In order to have an effective value of $2q/a$ around 1, N_2 must be greater than N_1 which implies that in the middle latitudes this instability will occur mainly when the mean static stability is unstable at certain periods of the day. This solution is also applicable for very low values of f and will define a secondary scale for these instabilities. Perhaps this case is very important with respect to cloud clusters found in the tropics which have scales of a few hundred kilometers. It may also be, as we will show in Part II, that this type of solution is strongly connected with the appearance of the low-level jet in the Great Plains.

b. A radiative condition at the top of the tropopause: Case B

In this case practically no reflection is observed and the growth behavior of the waves in the lower atmosphere is quite similar to that of Case A. For example, in the upper part of Fig. 9 we can see the contours of vertical velocity for the rigid boundary condition at $z=10{,}000$ m and in the lower part of Fig. 9 we have the corresponding solution for the radiation condition. The only noticeable difference is that the waves grow faster in the rigid boundary case.

A complete discussion of trapeze instability in an open domain was made by Fels (1973) in which he concluded that for very small values of N_1/N_0 the waves grow to a finite value in the lower boundary layer. However, when $N_1/N_0 \approx 1$ the waves will grow exponentially. Let us now briefly discuss these results.

If we multiply $\rho_0 V$ by Eqs. (2.1)–(2.3) and use (2.4), we can write the kinetic energy equation in the form

$$\left(\beta\rho_0\frac{V^2}{2}\right)t = -\nabla(\theta_0\rho_0 V\pi)+\rho_0\beta W\theta. \tag{4.7}$$

Then, by defining the potential energy as

$$P = +\tfrac{1}{2}\beta\rho_0 g\theta^2/\tilde{\theta}_z, \tag{4.8}$$

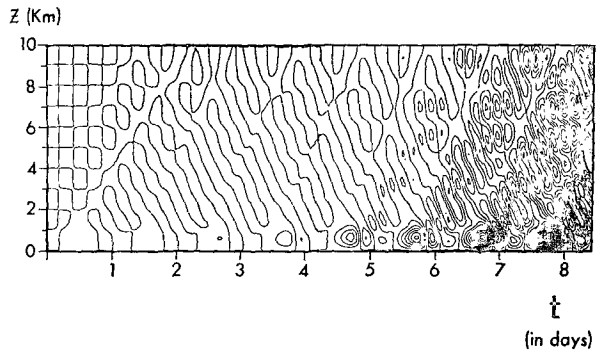

FIG. 8. As in Fig. 4 except for Case V and a contour interval of 0.1.

TABLE 1. Parameters used in Figs. 4–8.

Case	f (sec^{-1})	H_m	N_F	h_B	N_1	N_2	a^2	$2q/a$	λ_H (km)	Growth Period time (days)	T (hr)	Relative frequency
I	0	10^4	0.7×10^{-2}	10^3	0.7×10^{-2}	0.7×10^{-2}	1.0	1.0	392	5.5	48	$\omega_0/2$
II	0	10^4	0.7×10^{-2}	10^3	0.7×10^{-2}	0.63×10^{-2}	1.0	0.8	392	6.0	48	$\omega_0/2$
III	1×10^{-5}	10^4	1.0×10^{-2}	3×10^3	0.7×10^{-2}	0.7×10^{-2}	0.74	0.95	805	—	—	—
IV	1×10^{-5}	10^4	1.0×10^{-2}	3×10^3	0.7×10^{-2}	0.7×10^{-2}	0.94	0.96	628	3	48	$\omega_0/2$
V	1.2×10^{-4}	10^4	1.0×10^{-2}	10^3	0.3×10^{-2}	0.9×10^{-2}	11.24	0.80	174	1	16	$\frac{3}{2}\omega_0$

we can obtain the time variation of the potential energy by multiplying (2.5) by $\beta\rho_0 g\theta'/\theta_z$:

$$P_t=\left(\frac{\beta\rho_0 g\theta^2}{2\theta_z}\right)_t=-\beta\rho_0 g\theta W+\frac{\frac{1}{2}\beta\rho_0 g\theta^2}{2\bar{\theta}_z{}^2}\bar{\theta}_{zt}. \quad (4.8)$$

After taking the horizontal average (denoted by the bar), we add (4.7) and (4.8) and integrate through the height of the boundary layer ($z=h$). The result is the time variation of the wave energy which is expressed as

$$\int_0^h(\bar{K}+\bar{P})_t=-\theta_0\rho_0(\overline{W\pi})_h+\int_0^h\frac{\frac{1}{2}\beta\rho_0 g\bar{\theta}^2}{\theta_z{}^2}\bar{\theta}_{zz}dz. \quad (4.9)$$

The two terms on the right side of (4.9) have a simple interpretation: the first term is the work done by the pressure forces at the top of the boundary layer and the second the source of potential energy that drives the trapeze instability. Moreover, the intensity of this source depends on the value of (N_1/N_0). In view of Fels' results, when $N_1/N_0\ll1$ the work by pressure forces could balance the second term and no further energy increases will occur. However, when $N_1/N_0\approx1$ the energy source becomes so intense that the energy will keep growing which is in agreement with the numerical solutions.

Before ending this section let me show the effect of a stratification continuously varying with height; for this purpose we ran a case with

$$N^2=N_0{}^2+N_1{}^2[0.5-0.5\tanh\beta(z-h)]\cos\omega_0 t,$$

where $\beta=(1/250)$ m and $h=1500$ m. The solution for the first vertical wavenumbers $2\pi/h$ show no significant modification in comparison with the solution of the previous experiment. Fig. 10 shows the comparison between the potential temperature perturbation for the

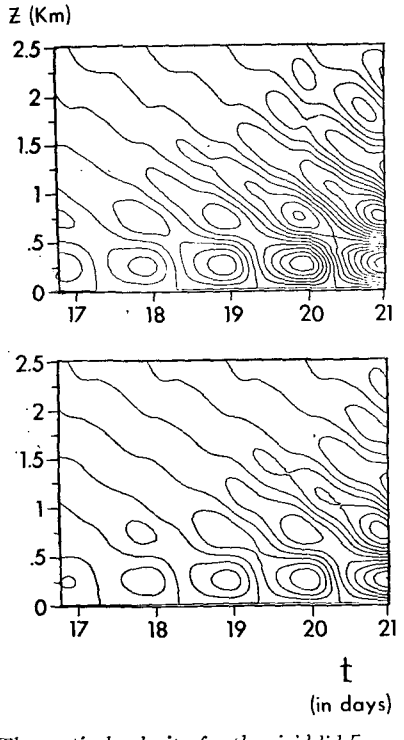

FIG. 9. The vertical velocity for the rigid lid [case A] (upper), and for Case B where the second derivative of w equals zero (lower). The parameters used for this latter case were $N_0{}^2=10^{-4}$ sec^{-2}, $(N_1/N_0)^2=0.9$ and $k=0.23\times10^{-4}$ m^{-1}.

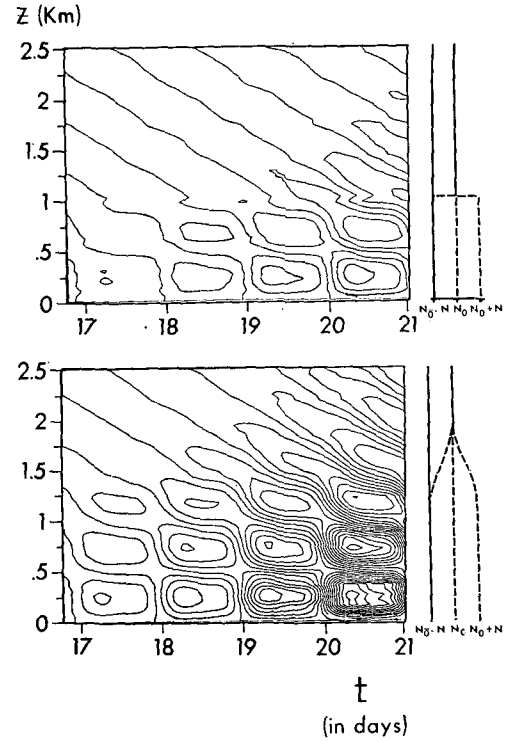

FIG. 10. Comparison of the potential temperature perturbations for the two different mean stratifications. The parameters used are the same as those described in Fig. 9.

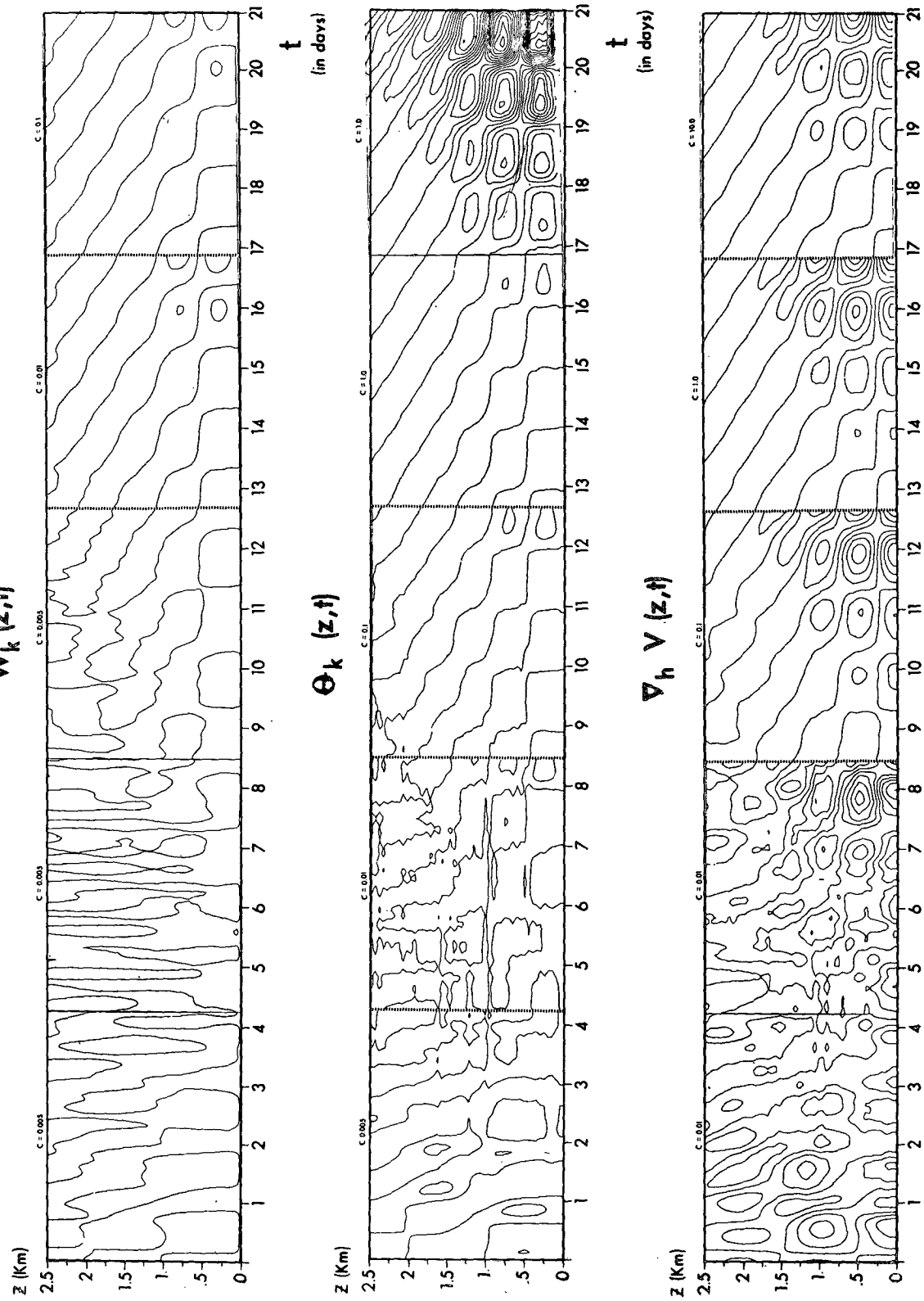

FIG. 11. The Fourier component of the vertical velocity, the perturbation potential temperature, and the horizontal divergence as a function of time and height. The parameters used are the same as those described in Fig. 9.

two different mean stratifications. Only the waves with higher vertical wavenumbers become more stable than those of the previous experiment. This indicates that the preferred waves will be those that have a vertical wavelength on the order of the height of the boundary layer. This fact will be accentuated by the viscous effect which will try to damp the waves with the larger wavenumbers.

Fig. 11 shows the perturbation potential temperature, the vertical velocity, and the horizontal divergence as a function of time and height. The wavenumber $k=0.23\times10^{-4}$ m^{-1}, $(N_1/N_0)^2=0.9$ and $N_0^2=10^{-4}$ sec^{-2}. The dashed lines indicate the region where the contour interval changes.

5. Conclusions

We can identify the diurnal oscillation of the atmospheric boundary layer as an important source of mesoscale internal gravity waves in the lower atmosphere.

The oscillation period of these waves is a function of latitude. A definitive two-day period may be found in the equatorial regions with scales on the order of a few hundred kilometers. In particular, a situation in which the mean stratification at any time of the day is unstable, the wavelength could be on the order of 100 km. In middle latitudes, however, a one-day oscillation will be the most predominant. Further studies of this type of instability including wind and moisture are underway and the results so far suggest that processes like the low-level jet and some cloud clusters are, in fact, generated by those waves. More observations that resolve the diurnal variation of the atmosphere are needed in order to verify the theoretical predictions and evaluate the importance of the generation of internal gravity waves by this process.

Acknowledgments. I would like to express my thanks to Mr. L. Polinsky for his assistance with the numerical program and general suggestions which helped to clarify the paper. I also thank Mrs. B. Williams and Mr. P. Tunison for typing the manuscript and preparing the figures.

REFERENCES

Bretherton, F. P., 1969: Momentum transport by gravity waves. *Quart. J. Roy. Meteor. Soc.*, **95**, 213–263.

Chapman, S., and R. S. Linzen, 1970: *Atmospheric Tides.* Dordrecht, Holland, Reidel Publ. Co., 200 pp.

Deardorff, J. W., G. E. Willis and D. K. Lilly, 1969: Laboratory investigation of non-steady penetrative convection. *J. Fluid Mech.*, **35**, 7–31.

Fels, S., 1973: The trapeze instability in an open domain. *J. Atmos. Sci.* (submitted for publication).

Gossard, E. E., J. H. Richter and D. Atlas, 1970: Internal waves in the atmosphere from high resolution radar measurements. *J. Geophys. Res.*, **75**, 3523–3536.

Lettau, H., and B. Davidson, 1957: *Exploring the Atmosphere's First Mile*, Vol. 2. New York, Pergamon Press, 202 pp.

Lilly, D. K., 1972: Wave momentum flux—a GARP problem. *Bull. Amer. Meteor. Soc.*, **53**, 17–23.

Murakami, M., 1972: Intermediate-scale disturbances appearing in the ITC zone in the tropical western Pacific. *J. Meteor. Soc. Japan*, **50**, 454–464.

Orlanski, I., 1968: Instability of frontal waves. *J. Atmos. Sci.*, **25**, 178–200.

——, 1973: Trapeze instability as a source of internal gravity waves. Part II. To be published.

Richtmyer, R. D., and K. W. Morton, 1967: *Difference Methods for Initial-Value Problems.* New York, Interscience, 405 pp.

Scorer, R. S., 1969: Billow mechanics. *Radio Sci.*, **4**, 1299–1308.

Venezian, G., 1969: Effect of modulation on the onset of thermal convection. *J. Fluid Mech.*, **35**, 243–254.

Yih, C.-S, and C.-H. Li, 1972: Instability of unsteady flows or configurations. Part 2. Convective instability. *J. Fluid Mech.*, **54**, 153–152.

Zaroodny, S. J., 1955: An elementary review of the Mathieu-Hill equation of real variable vase on numerical solutions. Memo. Rept. No. 878, Ballistic Research Laboratories, Aberdeen Proving Ground, Md., 31 pp.